

## MITIGATION OF HARMONIC CURRENT FOR BALANCED THREE-PHASE POWER SYSTEM BASED ON EXTENDED FRYZE ADAPTIVE NOTCH FILTER

SYAHRUL HISHAM MOHAMAD<sup>1,2,\*</sup>,  
MOHD AMRAN MOHD RADZI<sup>2</sup>, NASHIREN FARZILAH MAILAH<sup>2</sup>,  
NOOR IZZRI ABD. WAHAB<sup>2</sup>, AUZANI JIDIN<sup>1</sup>

<sup>1</sup>Advance Lightning, Power, and Energy Research (ALPER), Faculty  
of Engineering, Universiti Putra Malaysia (UPM), Malaysia

<sup>2</sup>Faculty of Electrical and Electronic Engineering Technology, Universiti  
Teknikal Malaysia Melaka (UTeM), Malaysia

\*Corresponding Author: syahrulhisham@utem.edu.my

### Abstract

The power quality problem, especially regarding harmonics contamination, has dramatically affected the overall power system stability. In response to this, using an Active Power Filter (APF) is considered one of the compelling methods to overcome harmonics issues. This paper presents the implementation of Shunt APF with an improved adaptive notch filter known as Extended Fryze Adaptive Notch Filter (EFANF) for fundamental signal extraction. The adaptive notch filter has improved the utilization from a single-phase to three-phase application for direct fundamental signal extraction and is designed to cater DC link voltage regulation controllers based on the power loss equation by applying Fryze current control power. This extraction algorithm inherits simple design construction and frequency tracking, eliminating PLL reliance on synchronization. The proposed algorithm also improved the design by eliminating the needs of low pass filter as others time domain algorithms. The algorithm's effectiveness in operation for the Shunt APF is validated through simulation using MATLAB/Simulink and experiment work by integrating the algorithm with DSPACE RS1104. Based on both evaluations, the results obtained show a satisfactory and reasonable agreement in mitigating the harmonics for multi-load conditions. Simulation and experimentally proven harmonics mitigation managed to reduce under 5% following the IEE standard, and the algorithm function within expectation for both steady and transient state conditions. In comparison between the simulation and experimental results, both results show almost similar results in terms of waveform for source voltage, source current, load current, and filter current in both steady state and transient state. In terms of THD values, both simulations and experimental results recorded that the THD values for both conditions are below 5%, where the range is 1.45% to 2.46% for simulation and 2.88% to 3.65% for experimental results. Furthermore, the DC link also tended to be maintained by the algorithm.

Keywords: Adaptive notch filter, Fryze, Harmonics, Shunt active power filter.

## 1. Introduction

The development of power systems has shaped multiple power generation, transmission, distribution, and application segments. All the advancements are often polluting and distorting the power system by increasing the utilization of non-linear loads, mainly contributed by power-electronics devices [1-3]. The need for power electronics devices can exponentially increase within the industrial and consumer sectors. Based on the extensive use of sensitive loads, such as computers and microprocessor-based industrial controllers, and now with the emergence of renewable energy such as solar and wind and the growth of electric vehicles, there is a growing need for effective harmonic measurement and compensation systems. Although conventional solutions have been used to mitigate power quality, such as passive filters in terms of harmonics, the solution is deemed ineffective, especially when involving load changes. As implementation of standard regulation in power flow is becoming more rigid such as IEEE519 and IEC 61000-3-2, active power compensation is seen as a better choice in realizing power quality (PQ) control.

Active power compensation offers better PQ compensation, especially harmonics, power factor, and active-reactive power control. Furthermore, the protection, management, performance, and efficiency of active power compensation are realized through continuous development in developing signal processing, detection, and extraction within mathematical algorithms and hardware throughout the past years. One of the apparatuses demonstrating a solid ability to eliminate harmonics is the Active Power Filter (APF) system. Such filters are an excellent way to reduce harmonic disturbances of voltage and current, sudden voltage fluctuations, transient disturbances, and current and voltage faults. Currently, there are multiple topologies of active power compensation available for additional compensation, such as series active power filter [4], shunt active power filter (SAPF), hybrid active power filter, and Unified Power Quality Conditioner (UPQC). Effective and efficient compensations are compulsory when dealing with harmonics' power quality. Hence, a precise algorithm is essential for extracting harmonics elements in controlling the power system's active power filter (APF). Over the years, various identification and extraction techniques have been developed; the methods can be divided into time and frequency domains.

The methods used in the frequency-based domain vary from commonly used fast Fourier and discrete Fourier algorithms, Kalman Filtering algorithm to wavelet transformation algorithm [5-7]. When using the mentioned techniques, most of the algorithms designed in the frequency domain require transformation, which is a little tedious to be applied in the time domain and usually incongruous with changing load in the power system. Another drawback of the frequency domain method is that it requires numerous cycles for better current estimation. In applying APF, the commonly used extraction method is usually within the time domain to cater to the changing waveform of loads in real-time situations, especially when involved with data acquisition. The time-domain techniques are divided into a few categories: classical methods derived from instantaneous power theory [8-10] and synchronous power theory [11-13], such as PQ, PQR, etc. DQ method. However, these methods usually involve multi-conversion planes and require additional filters to extract the information.

Another emerging method is the intelligent algorithms, which vary from the neural network, adaptive neural network, and adaptive linear neuron, where all these algorithms require training within the process [14-17]. Besides these three methods, another method used in the APF is the notch filter method, which is simple in design

and can accommodate changes in loads [18]. The work introduced adaptive notch filters as harmonics, interharmonics processing methods, and time-domain signal analysis [19]. However, the method is limited to only processing information due to the algorithm's lack of a controlling method for DC link control. Yazdani et al. also proposed the ANF for three-phase application [20], which performed harmonic reactive current extraction and harmonic decomposition. However, the work was limited to monitoring and extraction only. The ANF also been applied for ICC and DCC current control, but within this research also the DC Link control is not accounted for [21]. In some other works, the ANF replaces the lowpass filter function in the PQ algorithm for shunt APF [22-24] with a three-phase four-wire system. Although the strategy takes advantage of the transformation of the frame for instantaneous power flow, the application of ANF has increased the algorithm's complexity as the method includes the transformation process and integration of the ANF for filtering purposes. This strategy undermines the ANF's capability to directly filter the system's fundamental signal.

To utilize the potential of the ANF in shunt APF application. This paper presents an extended ANF application for harmonics extraction, DC link control, and current control. Within this method, three elements are focused on as the APF control system: the computational algorithm of reference current, the voltage regulation for the DC link control, and the generation of the firing pulse of the voltage source inverter (VSI). The main section of the paper is the proposed Extended Fryze Adaptive Notch Filter (EFANF) as the main algorithm component. The algorithm implements the Adaptive Notch Filter (ANF) as three-phase extraction algorithm where each block extract individual phase and the algorithm is implementing Fryze algorithm as current control and reference current generation where there this method applied minimization method in finding active and nonactive current calculation. Adjacent to the adaptive capability of the ANF, the algorithm also provides self-synchronization for the EFANF. This section also discusses the implementation of DC link voltage regulation, where the PI method is introduced as stability control within the EFANF, all highlighted in sections 2 and 3. The simulation and experimental works results are explained in section 4 of the paper. Finally, section 5 concludes the research contribution and highlights the overall significance of the impact of the work.

## 2. Principle Operation of Shunt APF

Shunt APF is implemented using a current control-voltage source inverter (CC-VSI), as shown in Fig. 1. The CC-VSI are connected in parallel with the non-linear loads through filter inductance. The CC-VSI performs the main task within the power quality system: inject (opposite magnitude) any unwanted harmonics current components produced due to the load current in the supply system at the point of common coupling (PCC). The instantaneous current source of the overall system is given in Eq. (1), where  $i_s(t)$  is the source current,  $i_L(t)$  is the load current and  $i_c(t)$  is the compensation current.

$$i_s(t) = i_L(t) - i_c(t) \quad (1)$$

Meanwhile, the instantaneous voltage source  $v_s(t)$  is given in Eq. (2), and the non-linear load current can be considered as the embodiment of fundamental current component and harmonics current components, as shown in Eq. (3)

$$v_s(t) = V_m \sin \omega t \quad (2)$$

$$i_L(t) = \sum_{n=1}^{\infty} I_n \sin(n\omega t + \phi_n) = I_1 \sin(\omega t + \phi_1) + \sum_{n=2}^{\infty} I_n \sin(n\omega t + \phi_n) \quad (3)$$

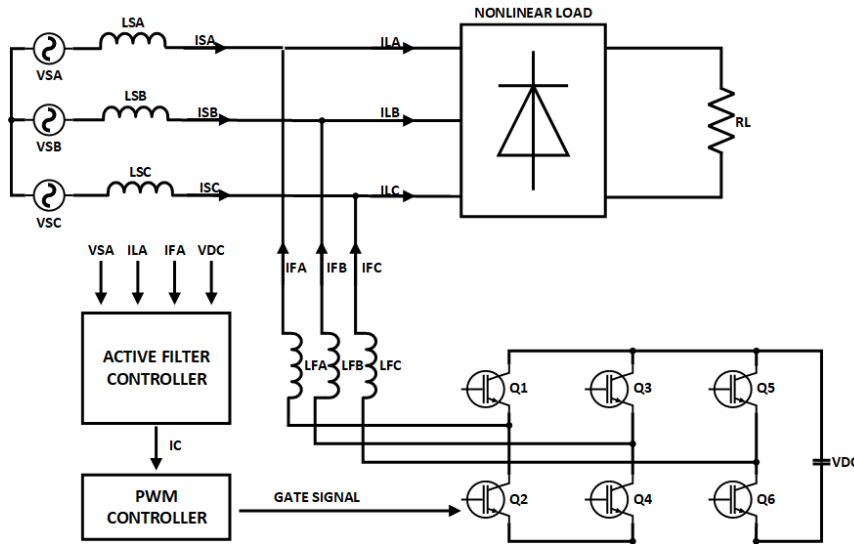


Fig. 1. Shunt APF system.

The instantaneous power of the load  $p_L(t)$  can be figured out based on Eq. (4) given as

$$p_L(t) = i_s(t) \times v_s(t) = V_m \sin^2 \omega t \times \cos \phi_1 + V_m I_1 \sin \omega t \times \cos \omega t \times \sin \phi_1 + V_m \sin \omega t (\sum_{n=2}^{\infty} I_n \sin(n\omega t + \phi_n)) = p_f(t) + p_r(t) + p_h(t) \quad (4)$$

The equation consists of active power  $p_f(t)$ , reactive power  $p_r(t)$ , and harmonics-induced power  $p_h(t)$ . Based on this, the real power drawn from the load is given in Eq. (5).

$$p_f(t) = V_m I_1 \sin^2 \omega t \times \cos \phi_1 \quad (5)$$

### 3. Principle of Current Control System

The structure of the current control system is shown in Fig. 2. The system can be divided into three major components. The first part is the computation of the reference current using an extended fryze adaptive notch filter (EFANF), the second part is the self-synchronization of the EFANF, and the third component is the DC link voltage regulation and the firing pulses for the APF.

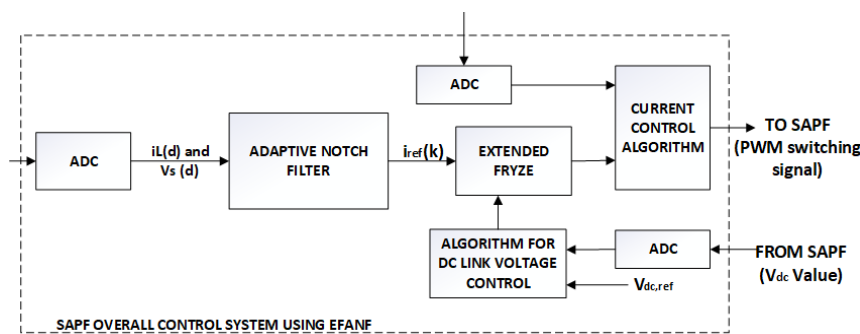


Fig. 2. Shunt APF system flow diagram.

### 3.1. Adaptive notch filter

Ideally, an adaptive notch filter (ANF) works in the concept of a linear gain applied for all the frequencies except a specified frequency where the frequency gain is zero. Based on this characteristic, the filter can withdraw an implicit signal of the sinusoidal waveform from the specified frequency's measured component of an electrical power system. ANF has well been researched in removing noises within the sinusoidal waveform [25]. Originally, ANF is based on an IIR filter [26]; however, with improvement in the notch frequency, the filter can adapt to notch frequency change with time by tracking the input signal frequency variation. This tracking capability eliminates the need for the signal frequency to be consistent, as is usually required for the typical notch filter to work efficiently. The ANF's dynamic operation can refer to the following set of differential equations.

$$\ddot{x} + \theta^2 x = 2\varepsilon\theta e(t) \quad (6)$$

$$\dot{\theta} = -\gamma x \theta e(t) \quad (7)$$

$$e(t) = u(t) - \dot{x} \quad (8)$$

The ANF can be composed of the following elements based on the differential equations. The input signal of the ANF is given by  $u(t)$ . The estimation frequency of the ANF system is given by  $\theta$ . The accuracy and convergence speed are determined by two coefficients within the ANF known as  $\gamma$  and  $\varepsilon$ . The two coefficients, however, must compensate each other for the ANF to work effectively and most efficiently,  $\dot{\theta}$  represents the updated law for the frequency estimation [27].

In a functional single sinusoidal input  $u(t) = A_1 \sin(\omega_0 t + \varphi_1)$ , the used ANF has an explicit characteristic where it has a unique periodic orbit located at  $O$  as shown in Eq. (9). For a single ANF system, three functional outputs will be produced by the ANF, which are the filtered cos signal noted by  $\bar{x}$  but in negative magnitude, filtered sin signal noted as  $\dot{\bar{x}}$  which is identified as the input signal and finally  $\bar{\theta}$  as the frequency of the signal.

$$O = \begin{pmatrix} \bar{x} \\ \dot{\bar{x}} \\ \bar{\theta} \end{pmatrix} = \begin{pmatrix} -A_1 \cos(\omega_0 t + \varphi_1) / \omega_0 \\ A_1 \sin \omega_0 (\omega_0 t + \varphi_1) \\ \omega_0 \end{pmatrix} \quad (9)$$

When involving a three-phase power system, for a shunt active power filter, the measurement of the waveform will apply three-phase waveforms of voltage and current for supply and load. Any three-phase sinusoidal voltage or current can be represented based on Eq. (10).

$$u(t) = \begin{pmatrix} u_a(t) \\ u_b(t) \\ u_c(t) \end{pmatrix} = \begin{pmatrix} A_a \sin(\omega t + \varphi_a) \\ A_b \sin(\omega t + \varphi_b) \\ A_c \sin(\omega t + \varphi_c) \end{pmatrix} \quad (10)$$

For the three-phase application, improvement can be applied to the ANF in terms of frequency tracking as the filter shares the common frequency  $\omega_0$  in the same electrical power system. Based on this, the frequency law of triple ANF can be shared, thus reducing the complexity of the ANF from the 9th order to the 7th order integration function. The ANF will work in parallel order in extracting the fundamental components by sharing the standard frequency over time. The fundamental equation of the ANF for a three-phase system can be nominated in Eqs. (11) to (13), where the

phase is represented as  $n$  for phases a, b, and c. Meanwhile, the updated law of frequency is based on the summation of the error signal of all three phases.

$$\ddot{x}_n + \theta^2 x_n = 2\varepsilon\theta e_n(t) \quad (11)$$

$$\dot{\theta} = -y\theta \sum x_n e_n(t) \quad (12)$$

$$e_n(t) = u_n(t) - \dot{x}_n \quad (13)$$

When the equation is expanded to the respective phase, the ANF phase error equation is given as Eq. (14), the error for each phase is inserted into Eq. (12), where the ANF phase update law is given as Eq. (15).

$$e_n(t) = \begin{pmatrix} e_a(t) \\ e_b(t) \\ e_c(t) \end{pmatrix} = \begin{pmatrix} u_a(t) - \dot{x}_a \\ u_b(t) - \dot{x}_b \\ u_c(t) - \dot{x}_c \end{pmatrix} \quad (14)$$

$$\begin{aligned} \dot{\theta} &= -y\theta \sum x_n e_n(t) = -y\theta(x_a e_a(t) + x_b e_b(t) + x_c e_c(t)) \\ &= -y\theta(x_a(u_a(t) - \dot{x}_a) + x_b(u_b(t) - \dot{x}_b) + x_c(u_c(t) - \dot{x}_c)) \\ &= -y(\theta x_a(u_a(t) - \dot{x}_a) + \theta x_b(u_b(t) - \dot{x}_b) + \theta x_c(u_c(t) - \dot{x}_c)) \end{aligned} \quad (15)$$

The ANF for each phase is given as Eq. (16), where  $\theta$  is obtained from the integration of  $\dot{\theta}$  and  $x$  obtained from the double integration of  $\ddot{x}$ .

$$\begin{pmatrix} ANF_a \\ ANF_b \\ ANF_c \end{pmatrix} = \begin{pmatrix} \ddot{x}_a + \theta^2 x_a = 2\varepsilon\theta e_a(t) \\ \ddot{x}_b + \theta^2 x_b = 2\varepsilon\theta e_b(t) \\ \ddot{x}_c + \theta^2 x_c = 2\varepsilon\theta e_c(t) \end{pmatrix} \quad (16)$$

### 3.2. Reference current estimation

In a three-phase power system, based on Eq. (4), the power flow within the system usually consists of absolute power, reactive power, and harmonics power. Therefore, the power term containing all efficient and non-efficient powers terms in the three-phase system is defined as Eq. (17).

$$S_e^2 = (3V_{e1}I_{e1})^2 + (3V_{e1}I_{eH})^2 + (3V_{eH}I_{e1})^2 + (3V_{eH}I_{eH})^2 \quad (17)$$

where  $(3V_{e1}I_{e1})^2$  refers to the fundamental effective apparent power and  $(3V_{e1}I_{eH})^2 + (3V_{eH}I_{e1})^2 + (3V_{eH}I_{eH})^2$  refers to nonfundamental effective apparent power. By applying ANF for the measured voltage and current, their fundamental components can be extracted, and the fundamental power for the system can be obtained based on the extracted components. Based on this, the estimation of the reference supply current will be produced. However, to ensure the successful task of SAPF, the DC link voltage needs to be controlled to ensure that it is maintained at the reference value. As the DC link of a SAPF acquires its power from the line and is accustomed to losses due to switches and active power transfer, the DC link voltage is exposed to various disturbances, leading to instability of the voltage. To be overwhelmed with this condition, a DC link control is essential to the SAPF. The DC-link reference is determined and compared with this system's measured DC link voltage. The error between the reference and measured DC link voltage is passed into the proportional-integral controller (PI). Loss is integrated into the instantaneous power equation, as in Eq. (18), where this is on the improvement point compared to previous works for ANF application SAPF.

$$\bar{p}_{3\phi} = v_a i_a + v_b i_b + v_c i_c + P_{dc} \tag{18}$$

The error or difference obtained from DC link voltage measurement is shown in Eq. (19), and the PI controller is applied towards the error to get the value as power losses of DC-link shown in Eq. (20).

$$e_{vdc}(t) = v_{dcref} - v_{dcsense} \tag{19}$$

$$P_{dc} = P_{dc}(t - 1) + K_p(e_{vdc}(t) - e_{vdc}(n - 1)) + K_i e_{vdc}(t) \tag{20}$$

Meanwhile, the three-phase reference supply is obtained through the fryze equation [28-31], where this method determines the reference current based on the average value of three-phase instantaneous power. The equivalent conductivity calculates the average current, and the average admittance is determined based on the concept of aggregate voltage as follows,

$$G_e = \frac{\bar{p}_{3\phi}}{V_{\Sigma}^2}, \quad \text{where } V_{\Sigma}^2 = \sqrt{v_a^2 + v_b^2 + v_c^2} \tag{22}$$

When the equation is expanded, the reference current can be given as,

$$i_{refk} = G_e v_k, \quad k = (a, b, c) \tag{23}$$

$$i_{refk} = \begin{bmatrix} i_{refa} \\ i_{refb} \\ i_{refc} \end{bmatrix} = \begin{bmatrix} \frac{(v_a i_a + v_b i_b + v_c i_c + P_{dc}) \times v_a}{\sqrt{v_a^2 + v_b^2 + v_c^2}} \\ \frac{(v_a i_a + v_b i_b + v_c i_c + P_{dc}) \times v_b}{\sqrt{v_a^2 + v_b^2 + v_c^2}} \\ \frac{(v_a i_a + v_b i_b + v_c i_c + P_{dc}) \times v_c}{\sqrt{v_a^2 + v_b^2 + v_c^2}} \end{bmatrix} \tag{24}$$

The individual reference current for each phase sequence can be obtained from Eq. (24).

#### 4. Result and Analysis

The performance of the proposed EFANF is verified by simulation and experimental works. Table 1 describes the parameters of design that are being applied in the simulation.

**Table 1. Simulation parameters.**

Parameter	Value
Source Voltage	415 V (RMS), 50 Hz
Source Impedance	1 Ω, 1 mH
DC Link Capacitance	3300 μF
DC Link Reference Voltage	700 V
Filtering Inductor	500 mH
ANF Gains	$\varepsilon = 0.16, \gamma = 180$
Non-linear load	Resistive Load
(3 Phase rectifier with 3 load conditions)	$R1 = 80 \Omega, R2 = 50 \Omega$ and $R3 = 36 \Omega$
	Resistive with Inductive Load
	$R1L1 = 77\Omega$ 30 mH,
	$R2L2 = 69\Omega$ 36 mH and
	$R3L3 = 41\Omega$ 41 mH
	Resistive with Capacitive Load
	$R1C1 = 65 \Omega$ 12 μF, $R2C2 = 65 \Omega$ 19 μF and $R3C3 = 65\Omega$ 36 μF

### 4.1. Simulation results

The performance, reliability, and efficiency of the EFANF for a balanced three-phase SAPF are initially simulated and evaluated using MATLAB-Simulink. According to the circuit shown in Fig. 3, inputs for the EFANF algorithm are based on the measured  $i_{sa}, i_{sb}, i_{sc}, i_{la}, i_{lb}, i_{lc}$  and the three-phase source voltage  $v_{sa}, v_{sb}, v_{sc}$  to come out with currents references  $i_{refa}, i_{refb}, i_{refc}$  for the APF. Evaluation is based on resistive load for three load conditions and tested for sudden changes of load for increasing and decreasing current and the keenness of the EFANF to succumb to the changes. The operation is tested to activate the APF after reaching a simulation time of 0.1s.

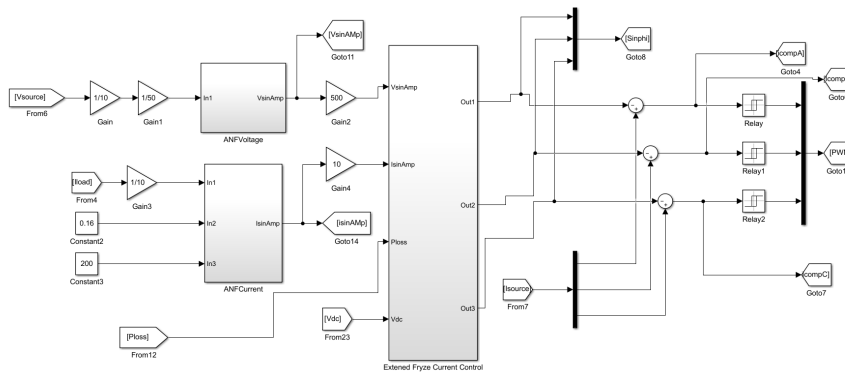
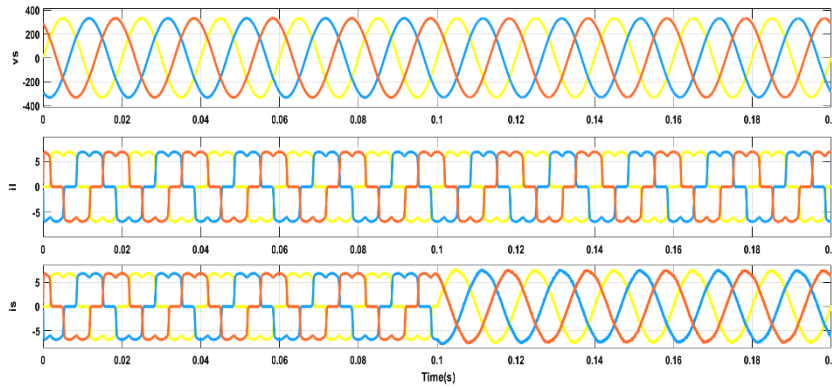


**Fig. 3. MATLAB simulation diagram for EFANF control system.**

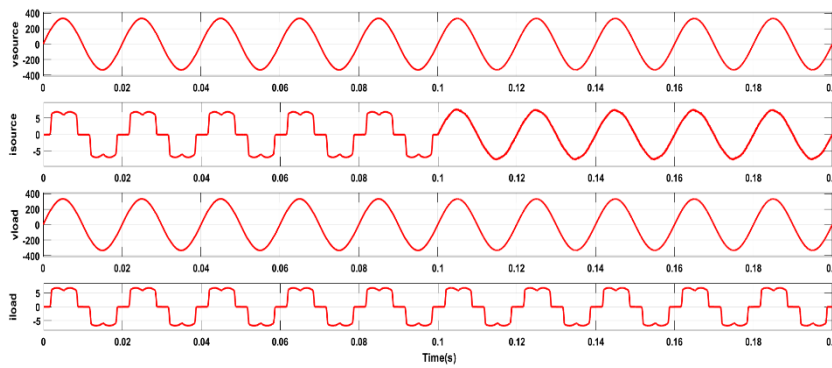
The system will be subjected to a non-linear rectifier with three different resistivity values for the output. Fig. 4 shows the output waveform of the power system connected with SAPF at the point of PCC. The measurement is taken before the PCC for source voltage ( $V_s$ ) and sources current ( $I_s$ ) and after the PCC for load voltage ( $V_l$ ) and load current ( $I_l$ ). As shown in Fig. 2, the system's voltage is a pure sinusoidal waveform, and the load is a distorted waveform due to the rectifier. Figure 5 focuses on phase-A waveforms for source voltage, source current, load voltage, and load current. To obtain the THD for the simulation, PowerGui FFT Analysis Tool MATLAB Simulink is used for immediate result. Based on the Fast Fourier Transform (FFT) analysis, it can be shown that the harmonics due to non-linear load are given in Fig. 7, where the THD value is 28.29 percent.

Based on Fig. 5, the current source waveform is being mitigated from the distortion by the SAPF. From point 0.1s, the load waveform has become sinusoidal, and at the same time, no distortion occurred within the source voltage and load voltage, and there is not also change that happened towards the load current. The APF is successfully mitigating the harmonics at the PCC. To evaluate the APF currents, details of the reference current, compensation current, and filter current are given in Fig. 6. It is shown that the EFANF managed to extract the fundamental current after three cycles of the waveform, and the compensation current is provided in Eq. (25).

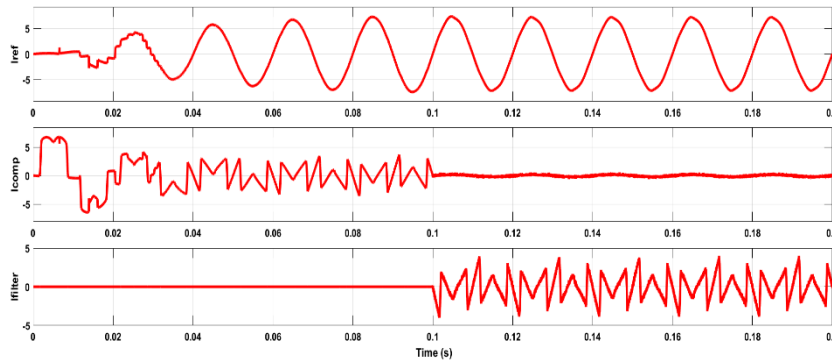
$$i_{comp} = i_{source} - i_{ref} \tag{25}$$



**Fig. 4. Simulation results of 80 Ω load for source voltage, load current, and source current before and after activation of APF.**



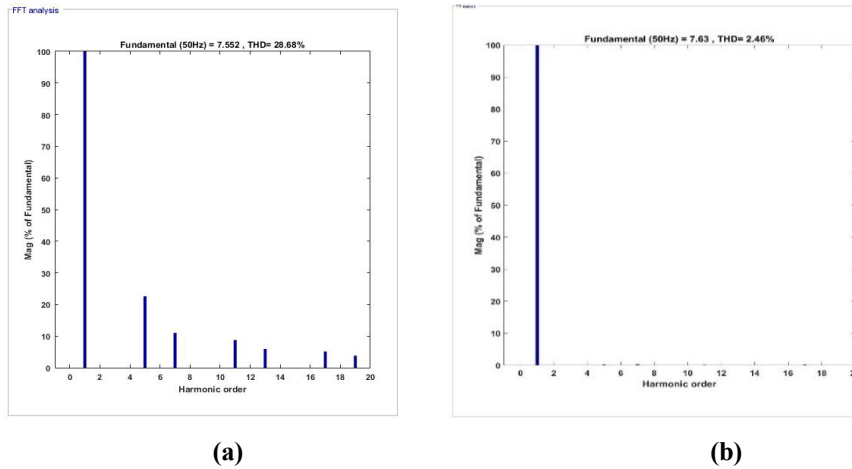
**Fig. 5. Simulation results for phase A before and after activation of APF.**



**Fig. 6. Simulation result for reference current, compensation current, and filter current before and after activating APF for phase a.**

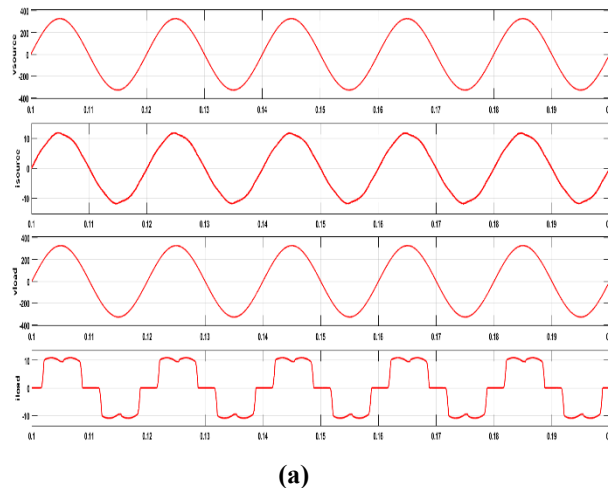
Figure 6 shows the waveform for the reference current, compensation current, and filter current for phase a. The ANF produces the reference current and inputs it into the APF current control. The difference between the reference and source current will have the required compensation current for the APF to mitigate the harmonics. At simulation time 0.1s, the APF is activated, and the filtering current

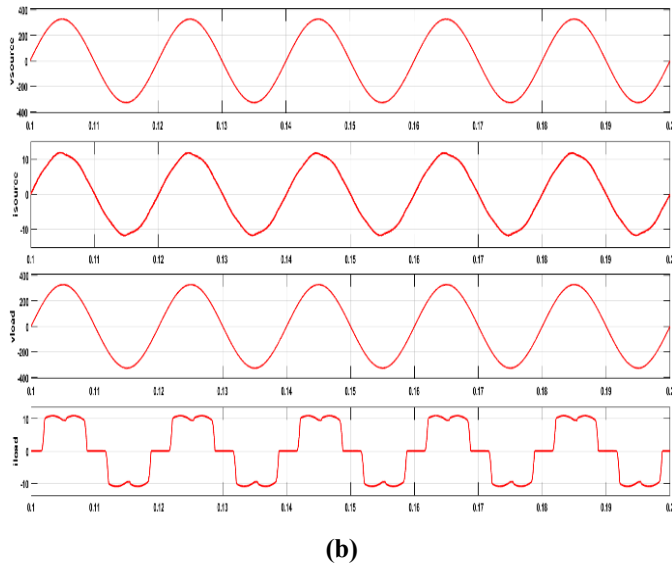
follows the required harmonics mitigation value for the load. The total harmonics distortion value of the source current after connecting APF is seen to reduce to 3.20 % due to the compensation current, as shown in Fig. 7.



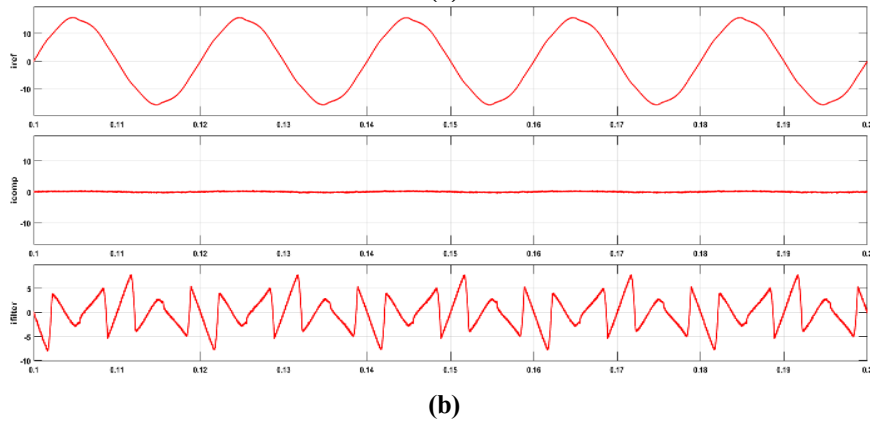
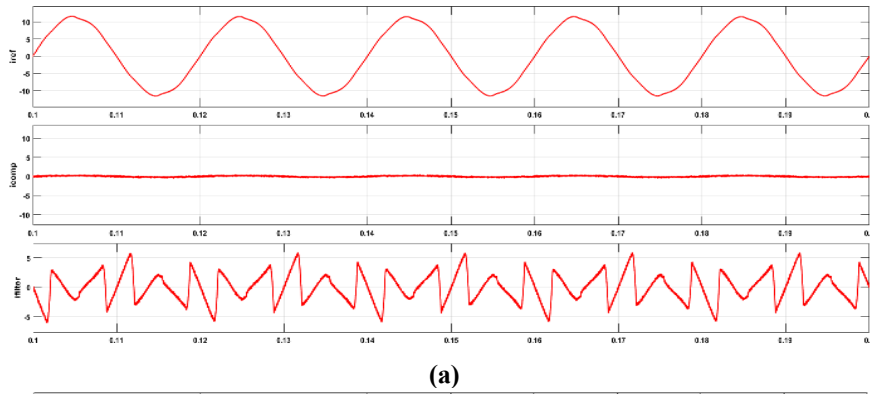
**Fig. 7. THD analysis for simulation of 80- $\Omega$  load (a) before connecting APF and (b) after connecting APF.**

Furthermore, the EFANF is simulated with two other stationary load conditions: resistive loads of 50 and 36 ohms, respectively. The waveforms of the voltage source, load current, and source current after compensation for both given loads are shown. In contrast, for investigated waveform for a single dedicated phase, a can be seen in Fig. 8. Based on the measured waveforms shown in Fig. 9, the EFANF provided the reference signal to the SAPF controller and mitigated the harmonics for all the stationary load conditions. The SAPF managed to bring down the THD from 28.29 % to 2.55% for 50- $\Omega$  load and 2.40% for 36- $\Omega$  load, respectively, as highlighted in the spectrum FFT analysis in Fig. 10. The obtained results confirm the capability of the EFANF in compensation purposes for operating SPAF to mitigate harmonics produced by the non-linear load system.

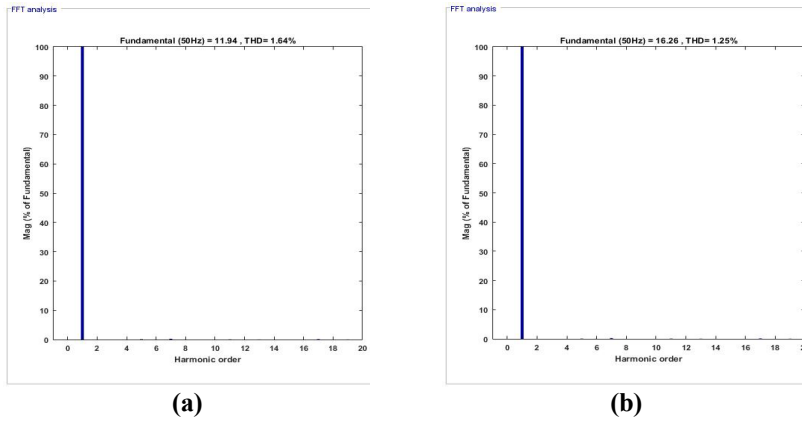




**Fig. 8. Simulation results of phase-a source voltage, source current, load voltage, and load current for (a) 50-Ω and (b) 36-Ω loads.**

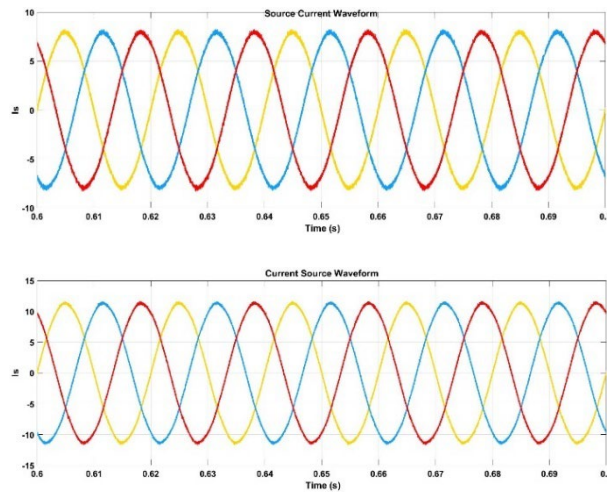


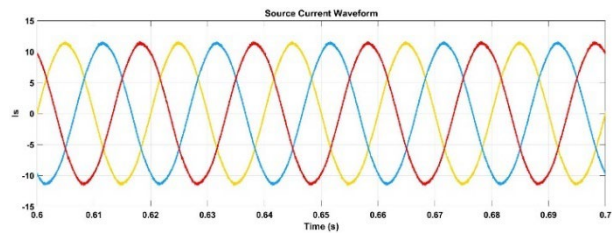
**Fig. 9. Simulation results of phase a reference current, compensation current, and reference current for (a) 50-Ω and (b)36-Ω loads.**



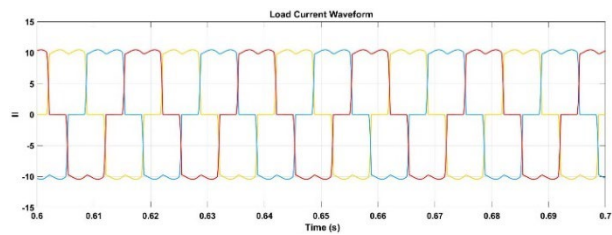
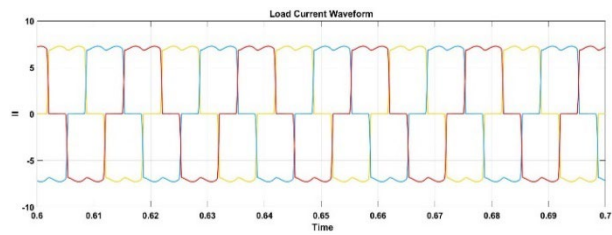
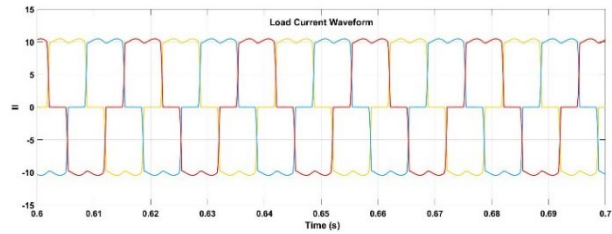
**Fig. 10. THD result after APF compensation for (a) 50 Ω and (b) 36 Ω loads.**

The proposed algorithm was also tested under different variations of loads for reactive power compensation under inductive and capacitive base loads to validate the adaptabilities of the algorithm in SAPF mitigation for the various waveform. Fig. 11 shows the result of the proposed EFANF for resistive with inductive load for three different loads, which are R1L1, R2L2, and R3L3 for source current, load current and filter current. On the other hand, Fig. 12 shows the source, load, and filter currents for three different resistive with capacitive loads given as R1C1, R2C2, and R3C3. Comparing the load current and source current for all three related loads, resistive with inductive and resistive with capacitive, shows that the EFANF can mitigate both reactive power compensation for resistive with inductive loads and resistive with capacitive loads. The THD values of the current source after mitigation for all loads are given as 2.41% for R1L1, 1.73% for R2L2, 1.25% for R3L3, 1.91% for R1C1, 2.09% for R2C2, and 2.54% for R3C3. Based on the given THD values, it can be proved that the EFANF can supply the SAPF effective reference current to reach the IEEE standard for the value of the harmonic below 5%.

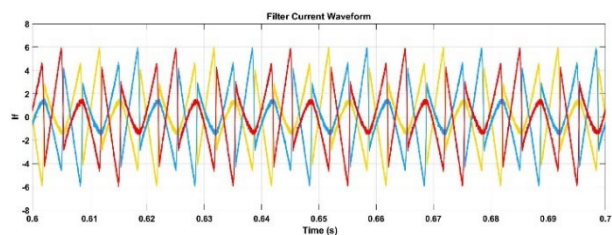
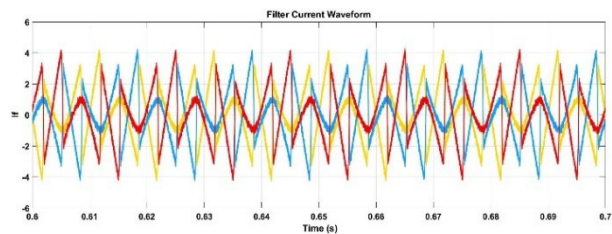


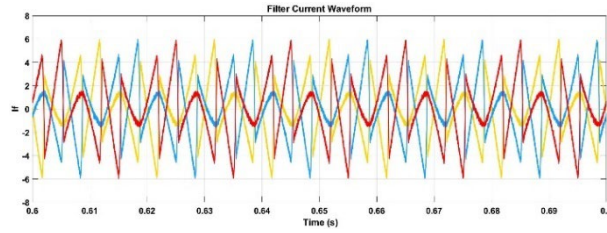


(a)



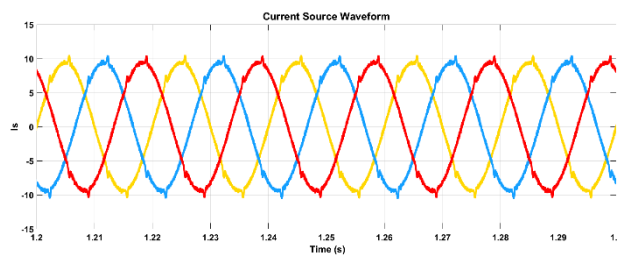
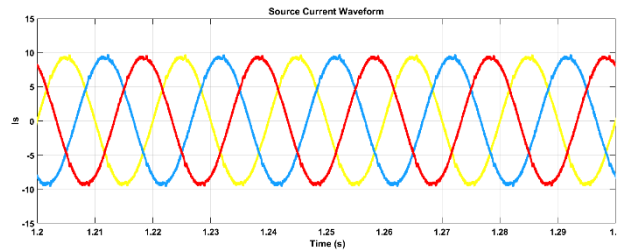
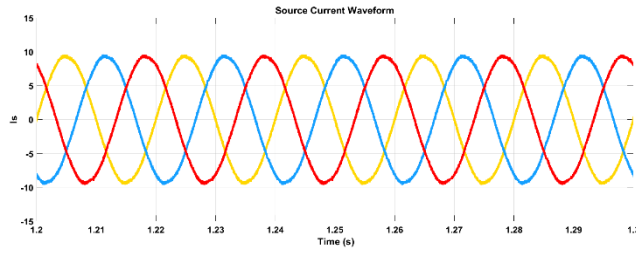
(b)



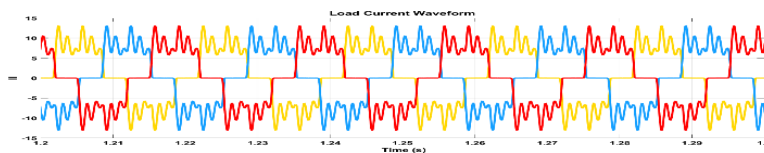
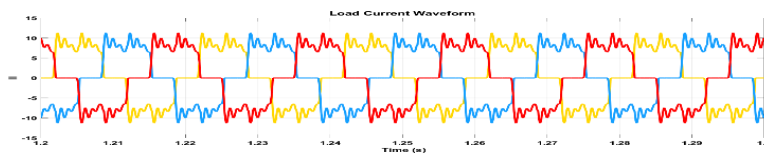


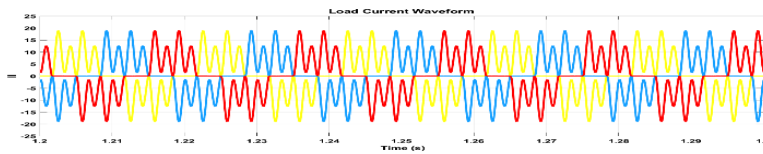
(c)

**Fig. 11. Simulation results of source current, load current and filter current for (a) R1L1, (b) R2L2, and (c) R3L3 loads.**

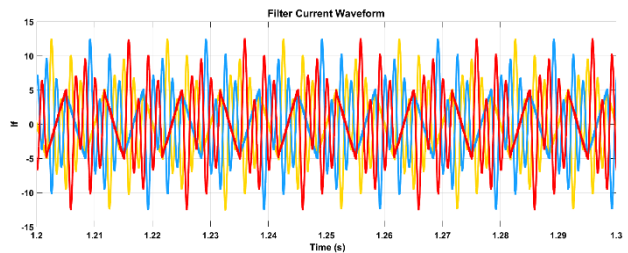
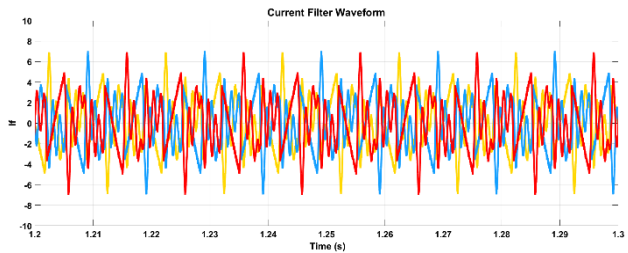
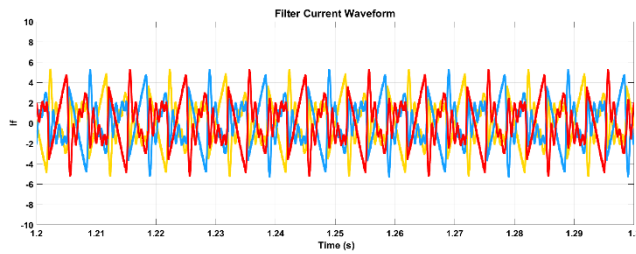


(a)





(b)



(c)

**Fig. 12. Simulation results of source current, load current, and filter current for (a) R1C1, (b) R2C2, and (c) R3C3 loads.**

Adaptableness of the EFANF is also being evaluated. The proposed algorithm is also simulated under a dynamic-state condition where the load will change between three resistivity load values that will directly affect the amount of current in the system. The dynamic changes are evaluated in changes of a resistive load from 82-Ω to 50-Ω and from 50-Ω to 36-Ω, where the changes will induce the increase of current changes. Figure 13 provides simulation results for both conditions with the voltage source, load current, and current source at transition points. It is shown that the EFANF managed to cater to the changes in load and respond to them immediately, whereas based on the figure, the EFANF required 0.05s to correspond to the changes.

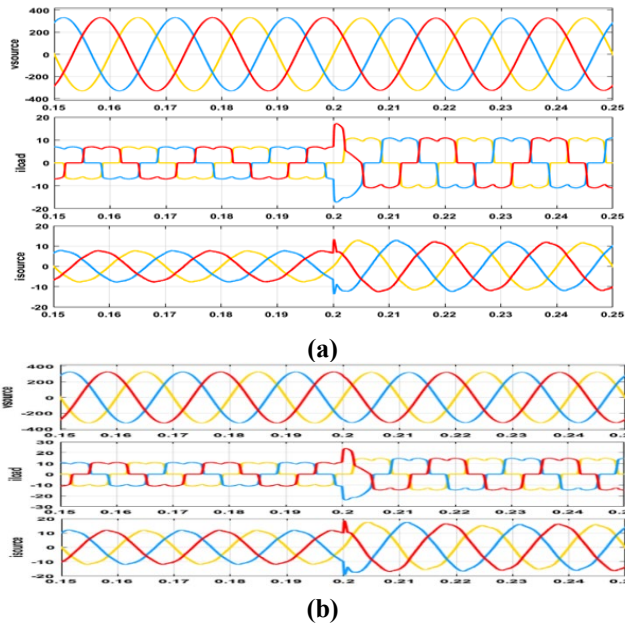


**Fig. 13. Simulation results of source voltage, load current, and source current under transient-state conditions for (a) 86-Ω to 50-Ω and (b) 50-Ω to 36-Ω.**

Furthermore, the EFANF adaptability to dynamic changes is also simulated for the loads' changes from 36 ohms to 50 ohms and 50 ohms to 82 ohms. The simulated waveforms are presented in Fig. 14 for both conditions, where the figure illustrates source voltage, load current, and source current. The findings confirmed the capability of the EFANF to produce the corresponding reference current within both stationary and transient conditions.

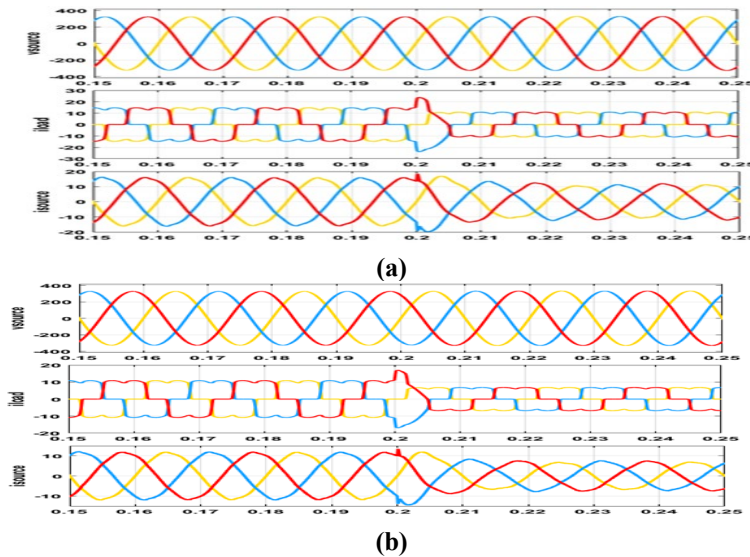


**Fig. 14. Simulated result of EFANF under dynamic changes for loads of (a) 36-Ω to 50-Ω and (b) 50-Ω to 82-Ω Re.**

### 4.2. Experimental results

A laboratory hardware setup was developed to validate the proposed algorithm. The hardware consisted of measurement circuits with current and voltage sensors, a three-phase inverter connected to the filtering inductor as APF, and DSPACE RS1104 as the controller, as shown in Fig. 15. A DSpace controller board is the connection point between the sensors and the output signals. For the APF, a three-phase inverter with DC-link is connected as the voltage source. The prominent role of the DSPACE is to implement the harmonics extraction algorithm, which will generate the reference current based on the EFANF. For the experiment, the supplied voltage of the system is set at 50Hz, 100 Vrms (line-to-line voltage). The experimental results of utilization of the proposed EFANF algorithm with PI DC-link control for resistive loads are shown in Fig. 16. The results include source voltage  $v_s$ , source current  $i_s$ , load current  $i_l$  and filter current  $i_{filter}$ .

The SAPF with EFANF effectively mitigates the harmonic current for the steady-state condition. The measurement is done using the Agilent DSO-X 2014A oscilloscope for the experimental result, covering source voltage, source current, load current, and filter current. In terms of THD calculation, the measurement is done by downloading the data from the oscilloscope. The data are then measured for harmonics decomposition using FFT analysis in MATLAB/Simulink.

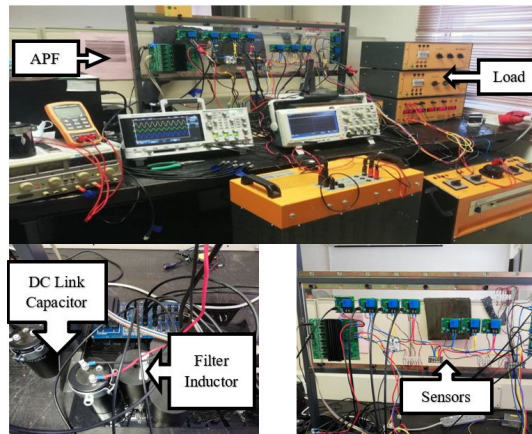


**Fig. 15. Laboratory hardware setup.**

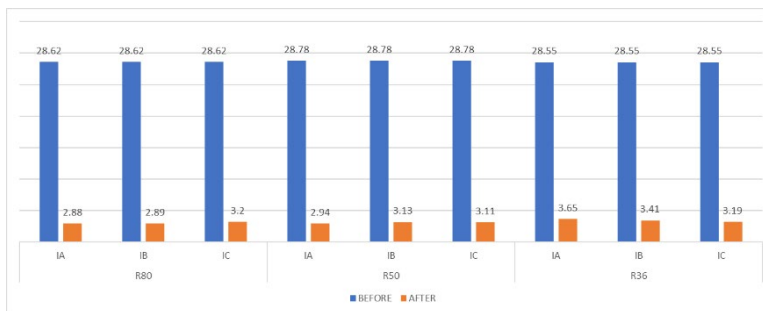


**Fig. 16. Experimental results of THD for three-phase source current after compensation.**

All harmonics are managed to be reduced below the required IEE standard, 5%. Nevertheless, the THDs of the three-phase supply current are monitored to see the algorithm's effectiveness in the experimental work, where the THD value can be seen in Fig. 16. From the results, the algorithm managed to reduce the harmonics of the source current with THD from 28.62% to 2.88%, 2.89% and 3.2% for 80 Ohms load, 28.77% to 2.94%, 3.13% and 3.11% for 50 Ohms load, lastly from 28.56% to 3.65%, 3.14% and 3.19% for 36 Ohms load regards to phase IA, IB and IC.

Figure 17 shows the waveforms of phase-a source voltage, source current, load current, and filter current in a steady-state condition obtained from experimental work. The source current waveform is sinusoidal and is in phase with the measured source voltage. Thus, THD is reduced for all the given loads, as shown in Fig. 17. The response of the proposed algorithm for steady-state conditions, when introduced to an inductive and capacitive load, is also confirmed with the experimental setup. The result is shown in Fig. 18, where it can be verified that the proposed algorithm can mitigate resistive with inductive loads for values R1L1, R2L2, and R3L3. After mitigation, the source current loads THD are given as 2.70%, 2.63%, and 2.78%, respectively.

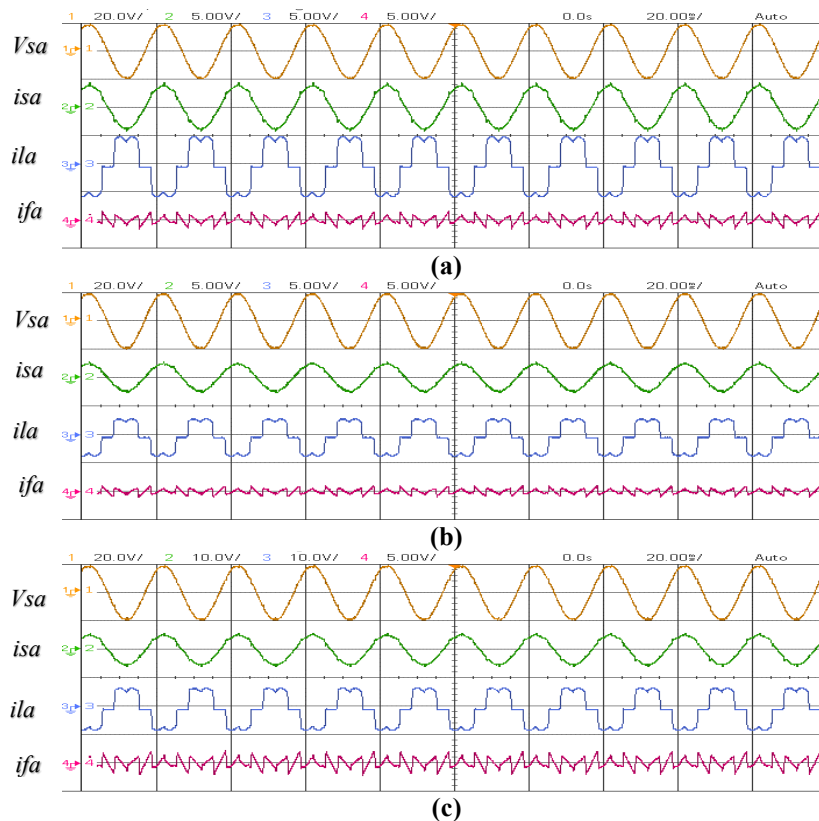


**Fig. 17. Experimental results of source voltage, source current, load current, filter current and THD values for (a) 82- $\Omega$  (b) 50- $\Omega$  and (c) 36- $\Omega$  loads.**

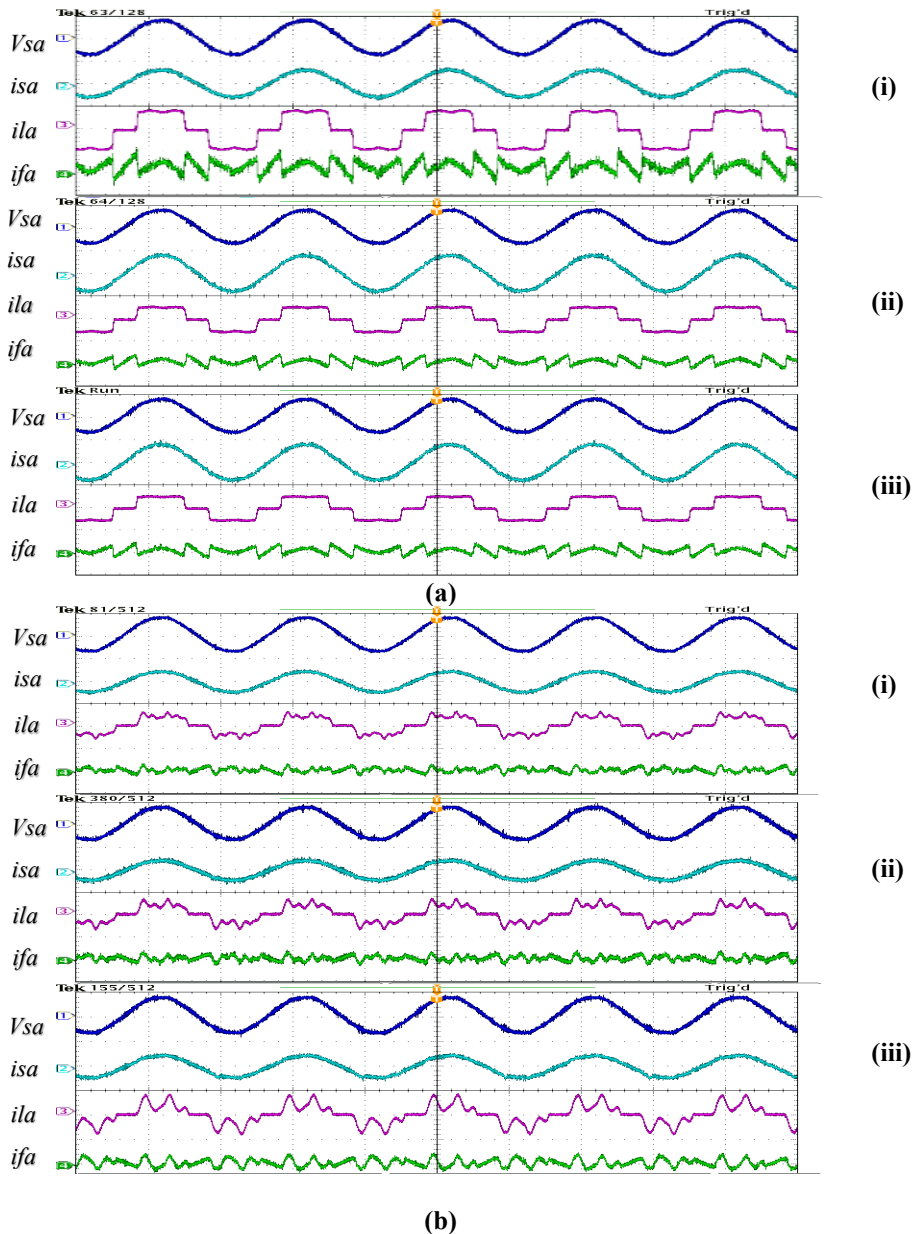


**Fig. 18. Experimental results of source voltage, source current, load current, filter current and THD values for (a-i) 67-Ω and 30H, (a-ii) 69-Ω and 36H, (a-iii) 76-Ω and 41H loads, (b-i) 60-Ω 12uF, (b-ii) 60-Ω 17uF and (b-iii) 60-Ω 36uF loads.**

The resistive with capacitive loads values of R1C1, R2C2, and R3C3. The values are within the required IEEE standard. THD's mitigated source current values are 2.52%, 2.99%, and 5.00% for each load. Based on these values, it can be concluded that the proposed EFANF algorithm can produce the appropriate reference current for the SAPF to work effectively. The SAPF also seems to have better stabilities for the

resistive and inductive loads than capacitive loads. However, in terms of mitigation, the EFANF can mitigate all the different types of loads in the experimental setup.

The effectiveness and feasibility of the proposed algorithm were also verified for transient-state operation during load-changing conditions. Figure 19 shows the state for reducing load capacity, which causes ascending current state, Fig. 19 also shows the increased load capacity, which causes descending current state. In both states, the EFANF managed to mitigate within 20ms for all load changes.

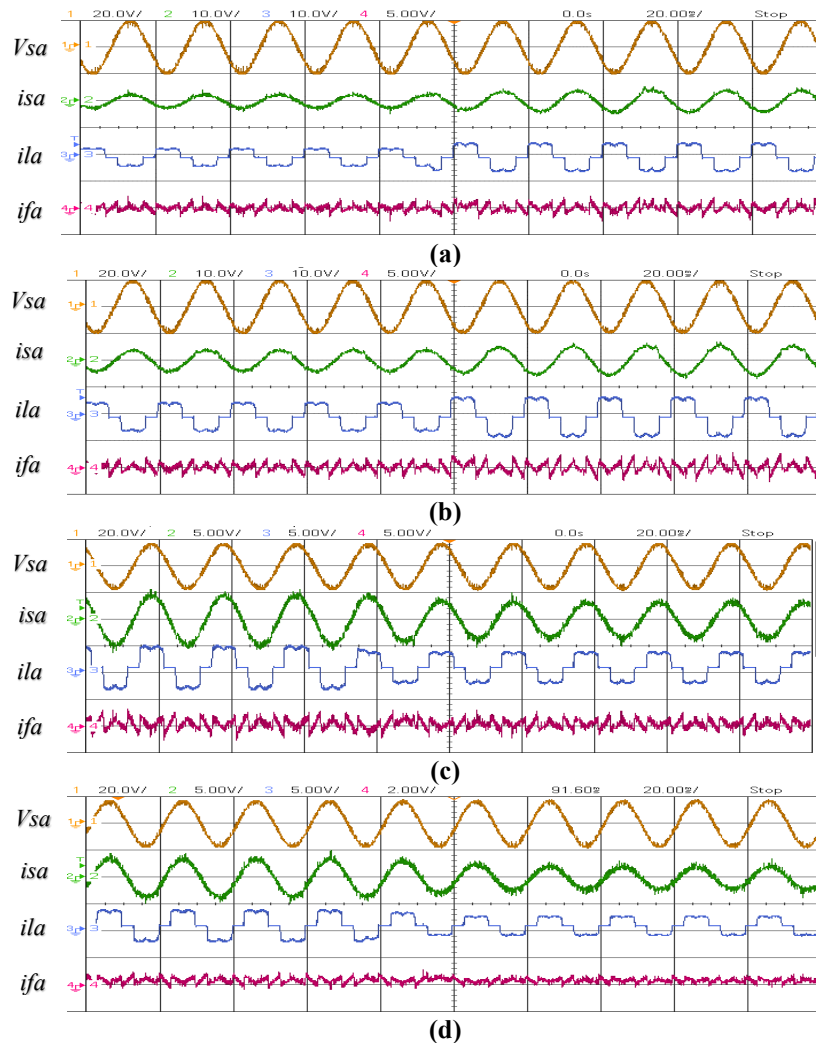


**Fig. 19. Experimental results of source voltage, source current, load current, filter current, and DC-Link voltage during transient-state conditions of (a) 82- $\Omega$  to 50- $\Omega$  (b) 50- $\Omega$  to 36- $\Omega$  (c) 82- $\Omega$  to 50- $\Omega$  and (d) 50- $\Omega$  to 36- $\Omega$ .**

In comparison between the simulation and experimental results, both results show almost similar results in terms of waveform for source voltage, source current, load current, and filter current in both steady state and transient state. In terms of THD values, both simulations and experimental results recorded that the THD

values for both conditions are below 5%, where the range is 1.45% to 2.46% for simulation and 2.88% to 3.65% for experimental results.

## 5. Conclusions

This paper presents the EFANF extraction algorithm utilized in SAPF to compensate for current harmonics in the three-phase three-wire system. The proposed algorithm demonstrated its capability to generate the reference current based on the notch filtering technique, as shown in both simulation results in MATLAB/Simulink and experimental work based on the validation with DSPACE RS1104. As the EFANF is self-synchro based on frequency adaptability, PLL is not required. The algorithm extracted the fundamental component and mitigated harmonics in balanced load conditions based on the analyses of steady-state and transient state conditions. The performance of the proposed algorithm has also been verified for different types and values of reactive loads both in simulation and experimental works.

The design of the EFANF also gives an optional improvement on the DC link voltage control algorithm as the losses of the DC link is provided as power losses within the system. In terms of performance, the EFANF managed to produce the THD according to the requirement of the IEE standard. Furthermore, the algorithm can adapt to the different types of loads. However, in the adaptation of EFANF, the algorithm is still dependent on two coefficients  $\gamma$  and  $\varepsilon$  for the algorithm to be working effectively. In current works, the coefficients are obtaining through empirical method. To improve the effectiveness of coefficients, future works are recommended to obtain the best possible coefficients values through optimization method.

## Acknowledgements

The authors would like to express their sincere gratitude to the Universiti Teknikal Malaysia Melaka (UTeM), Ministry of Education Malaysia, Universiti Putra Malaysia (UPM) and ALPER UPM and for the technical and financial support of this research.

### Nomenclatures

$3V_{e1}I_{e1}$	Fundamental effective apparent power
$3V_{eH}I_{eH}$	Harmonics power
$G_e$	The equivalent conductivity
$\overline{i_{refa}}, \overline{i_{refb}}, \overline{i_{refc}}$	Generated reference current phase a, b and c Ampere
$i_{sa}, i_{sb}, i_{sc}$	Current source phase a, b and c, Ampere
$v_{sa}, v_{sb}, v_{sc}$	Voltage source phase a, b and c, Volt
$\gamma$	Accuracy coefficients

### Greek Symbols

$\varepsilon$	Convergence speed coefficients
$\theta$	Estimation Frequency
$\hat{\theta}$	Updated law for the frequency estimation
$\omega_0$	Reference frequency

**Abbreviations**

APF	Active Power Filter
EFANF	Extended Fryze Adaptive Notch Filter
SAPF	Shunt Active Power Filter
THD	Total Harmonics Distortion

**References**

- Zare, F.; Soltani, H.; Kumar, D.; Davari, P.; Delpino, H.A.M.; and Blaabjerg, F. (2017). Harmonic emissions of three-phase diode rectifiers in distribution networks. *IEEE Access*, 5, 2819-2833.
- Alizade, A.; and Noshahr, J.B. (2017). Evaluating noise and DC offset due to inter-harmonics and supra-harmonics caused by back-to-back converter of (DFIG) in AC distribution network. *CIREN - Open Access Proceedings Journal*, 2017(1), 629-632.
- Patil, K.D.; and Gandhare, W.Z. (2011). Effects of harmonics in distribution systems on temperature rise and life of XLPE power cables. *Proceedings of the 2011 International Conference on Power and Energy Systems*, Chennai, India, 1-6.
- Toumi, T.; Allali, A.; Meftouhi, A.; Abdelkhalek, O.; Benabdelkader, A.; and Denai, M. (2020). Robust control of series active power filters for power quality enhancement in distribution grids: Simulation and experimental validation. *ISA Transactions*, 107, 350-359.
- Sundaram, E.; and Venugopal, M. (2016). On design and implementation of three phase three level shunt active power filter for harmonic reduction using synchronous reference frame theory. *International Journal of Electrical Power & Energy Systems*, 81, 40-47.
- Liu, H.; Hu, H.; Chen, H.; Zhang, L.; and Xing, Y. (2018). Fast and flexible selective harmonic extraction methods based on the generalized discrete Fourier transform. *IEEE Transactions on Power Electronics*, 33(4), 3484-3496.
- Panigrahi, R.; and Subudhi, B. (2017). Performance enhancement of shunt active power filter using a Kalman filter-based  $H_\infty$  control strategy. *IEEE Transactions on Power Electronics*, 32(4), 2622-2630.
- Jayasankar, V.N.; and Vinatha, U. (2020). Backstepping controller with dual self-tuning filter for single-phase shunt active power filters under distorted grid voltage condition. *IEEE Transactions on Industry Applications*, 56(6), 7176-7184.
- Harirchi, F.; and Simões, M.G. (2018). Enhanced instantaneous power theory decomposition for power quality smart converter applications. *IEEE Transactions on Power Electronics*, 33(11), 9344-9359.
- Liu, Y.-W.; Rau, S.-H.; Wu, C.-J.; and Lee, W.-J. (2018). Improvement of power quality by using advanced reactive power compensation. *IEEE Transactions on Industry Applications*, 54(1), 18-24.
- Chebabhi, A.; Fellah, M.K.; Kessal, A.; and Benkhoris, M.F. (2016). A new balancing three level three dimensional space vector modulation strategy for three level neutral point clamped four leg inverter based shunt active power filter controlling by non-linear back stepping controllers. *ISA Transactions*, 63, 328-342.

12. Naderipour, A.; Abdul-Malek, Z.; Ramachandaramurthy, V.K.; Kalam, A.; and Miveh, M.R. (2019). Hierarchical control strategy for a three-phase 4-wire microgrid under unbalanced and non-linear load conditions. *ISA Transactions*, 94, 352-369.
13. Hoon, Y.; Zainuri, M.A.A.M.; Al-Ogaili, A.S.; Al-Masri, A.N.; and Teh, J. (2021). Active power filtering under unbalanced and distorted grid conditions using modular fundamental element detection technique. *IEEE Access*, 9, 107502-107518.
14. Hou, S.; Fei, J.; Chen, C.; and Chu, Y. (2019). Finite-time adaptive fuzzy-neural-network control of active power filter. *IEEE Transactions on Power Electronics*, 34(10), 10298-10313.
15. Hou, S.; Fei, J.; and Chu, Y. (2018). Nonsingular terminal sliding mode control of active power filter. *Proceedings of the 2018 37<sup>th</sup> Chinese Control Conference (CCC)*, Wuhan, China, 2982-2987.
16. Tan, K.-H.; Lin, F.-J.; and Chen, J.-H. (2018). DC-Link voltage regulation using RPFNN-AMF for Three-Phase active power filter. *IEEE Access*, 6, 37454-37463.
17. Merabet, L.; Saad, S.; Abdeslam, D.O.; and Merckle, J. (2017). Direct neural method for harmonic currents estimation using adaptive linear element. *Electric Power Systems Research*, 152, 61-70.
18. Singh, B.; Kant, K.; and Arya, S.R. (2015). Notch filter-based fundamental frequency component extraction to control distribution static compensator for mitigating current-related power quality problems. *IET Power Electronics*, 8(9), 1758-1766.
19. Kewat, S.; and Singh, B. (2019). Modified amplitude adaptive control algorithm for power quality improvement in multiple distributed generation system. *IET Power Electronics*, 12(9), 2321-2329.
20. Yazdani, D.; Bakhshai, A.; and Jain, P. (2009). A three-phase approach to harmonic and reactive current extraction and harmonic decomposition. *Proceedings of the 2009 35<sup>th</sup> Annual Conference of IEEE Industrial Electronics*, Porto, Portugal, 3205-3210.
21. Mohamad, S.H.; Radzi, M.A.M.; Mailah, N.F.; Wahab, N.I.A.; Jidin, A.; and Lada, M.Y. (2020). Adaptive notch filter under indirect and direct current controls for active power filter. *Bulletin of Electrical Engineering and Informatics*, 9(5), 1794-1802.
22. Chilipi, R.S.R.; Al Sayari, N.; Al Hosani, K.H.; and Beig, A.R. (2017). Adaptive notch filter-based multipurpose control scheme for grid-interfaced three-phase four-wire DG inverter. *IEEE Transactions on Industry Applications*, 53(4), 4015-4027.
23. Dinh, N.D.; Tuyen, N.D.; Fujita, G.; and Funabashi, T. (2015). Adaptive notch filter solution under unbalanced and/or distorted point of common coupling voltage for three-phase four-wire shunt active power filter with sinusoidal utility current strategy. *IET Generation, Transmission & Distribution*, 9(13), 1580-1596.
24. Tuyen, N.D.; Fujita, G.; Funabashi, T.; and Nomura, M. (2012). Adaptive notch filter for synchronization and islanding detection using negative-

- sequence impedance measurement. *IEEJ Transactions on Electrical and Electronic Engineering*, 7(3), 240-250.
25. Mojiri, M.; and Bakhshai, A.R. (2007). Stability analysis of periodic orbit of an adaptive notch filter for frequency estimation of a periodic signal. *Automatica*, 43(3), 450-455.
  26. Mojiri, M.; and Bakhshai, A.R. (2004). An adaptive notch filter for frequency estimation of a periodic signal. *IEEE Transactions on Automatic Control*, 49(2), 314-318.
  27. Mojiri, M.; Karimi-Ghartemani, M.; and Bakhshai, A. (2010). Processing of harmonics and interharmonics using an adaptive notch filter. *IEEE Transactions on Power Delivery*, 25(2), 534-542.
  28. Nie, X.; and Liu, J. (2019). Current reference control for shunt active power filters under unbalanced and distorted supply voltage conditions. *IEEE Access*, 7, 177048-177055.
  29. Teshome, D.K.; Huang, T.D.; and Lian, K.-L.(2016). Distinctive load feature extraction based on Fryze's time-domain power theory. *IEEE Power and Energy Technology Systems Journal*, 3(2), 60-70.
  30. Kesharvani,, S.K.; Singh, A.; and Badoni, M. (2014). Conductance based fryze algorithm for improving power quality for non-linear loads. *Proceedings of the 2014 International Conference on Signal Propagation and Computer Technology (ICSPCT 2014)*, Ajmer, India, 703-708.
  31. Zeng, Z.; Zhao, R.; and Yang, H. (2014). Coordinated control of multi-functional grid-tied inverters using conductance and susceptance limitation. *IET Power Electronics*, 7(7), 1821-1831.